STABLE PTYCHOGRAPHIC PHASE RETRIEVAL VIA LOST SUBSPACE COMPLETION

Oleh Melnyk
Mathematical Imaging and Data Analysis, ICT
Helmholtz Center Munich
and
Department of Mathematics
Technical University of Munich
Munich, Germany
oleh.melnyk@tum.de

Anton Forstner
Department of Mathematics
Technical University of Munich
Munich, Germany
anton.forstner@tum.de

Felix Krahmer
Department of Mathematics
Technical University of Munich
Munich, Germany
felix.krahmer@tum.de

Nada Sissouno
Mathematical Imaging and Data Analysis, ICT
Helmholtz Center Munich
and
Department of Mathematics
Technical University of Munich
Munich, Germany
sissouno@ma.tum.de

***Abstract*—In this paper, we consider a special case of the phase retrieval problem called ptychography. Its is a popular technique of imaging, based on local illuminations of a specimen and further reconstruction from the far field diffraction patterns. The stability and success of the recovery process is heavily based on the choice of the illumination function commonly called a window. It describes the distribution of the light along the measured region. While for some windows the conditioning can be controlled, many important classes of windows, such as Gaussian windows, were not covered. We present a subspace completion method, which allows for a well-conditioned reconstruction for a much wider choice of windows, including Gaussian windows.**

***Index Terms*—phase retrieval, ptychography, regularization.**

I. Introduction

Phase retrieval is the problem of recovering a vector $x_0 \in \mathbb{C}^d$ from measurements given by

$$y_j = |\langle x_0, a_j \rangle|^2 + n_j, \ j = 1, \dots, J.$$

where a_j are called measurement vector. Due to the absolute value in the measurements, x_0 cannot be reconstructed uniquely and one can at best recover an equivalence class of objects $\{e^{i\theta} x_0 : \ \theta \in [0, 2\pi]\}$; the angle θ is commonly referred to as a global phase factor.

FK acknowledges support by the German Science Foundation DFG in the context of an Emmy Noether junior research group (project KR 4512/1-1). OM has been supported by the Helmholtz Association (project Ptychography 4.0).

In recent years, a special case of the phase retrieval problem called ptychography became popular in the scientific community. A full illumination of a specimen x_0 is replaced by a focused X-ray beam so that only a small region of the object is illuminated. Then a CCD camera captures the intensity of the resulting far field diffraction pattern. After taking these measurements, the object is shifted and another region is illuminated. The redundancy resulting from the overlapping regions allows to reconstruct the object from the collected intensities.

The obtained far field diffraction patterns are the squared amplitudes of the short-time Fourier transform corresponding to the illumination density. Since the images are pixelized, we consider a discretization of the measurements provided by the following equation

$$(y_\ell)_j = \left| \sum_{n=1}^{d} w_n (x_0)_{n+\ell} e^{-\frac{2\pi i (j-1)(n-1)}{d}} \right|^2 + n_{j,\ell}, \qquad (1)$$

for all $(j, \ell) \in [d] \times P$. The set $P \subset \{0, 1, \dots, d-1\}$ is the set of shifts of the object, $n_{j,\ell}$ is noise, $w \in \mathbb{C}^d$ is a localized illumination or window function, and $1 \leq \delta \leq d$ denotes its support size, i.e., $\mathrm{supp}(w) \subseteq [\delta]$. The notation $[n]$ is short for the set $\{1, \dots, n\}$.

Ptychography was introduced back in 1969 by Hoppe [1] and in the following years it was mostly developed by Rodenburg and coauthors [2]–[4]. Later it was rediscovered by the synchrotron community in the late 2000th, which resulted in

many practical applications. For instance, ptychography was used to image the internal structure of silk fibers [5], the 3D pore structure of a catalyst [6], and to visualize hair cells in the inner ear, called stereocilia, which are necessary for hearing and balancing and have a diameter that lies in the nanometre range [7].

The reconstruction of the object is commonly performed by one of the following iterative algorithms: versions of the *Alternating Projections* method developed by Gerchberg and Saxton [8] and Fienup [9], gradient descent schemes such as *Wirtinger Flow* [10] and the *Extended Ptychographic Iterative Engine* [11] developed specifically for ptychography. Although all of the mentioned algorithms are based on simple iterations, they possess several yet unresolved issues. Either the global convergence is not proven and good reconstruction is heavily dependent on a good initial guess or the time required by computations is too long. Thus, it remains an active topic of ongoing research to develop new non-iterative techniques. One such algorithm is Block Phase Retrieval (*BlockPR*) [12], which is also at the core of this paper and explained in detail in the next section. As for most algorithms, the stability of reconstruction with *BlockPR* strongly depends on the choice of the illumination function and is not yet understood for many important classes of windows. In this paper, we develop a modification of *BlockPR*, which significantly extends the range of allowed windows, including Gaussian windows as frequently used on practice.

II. Preliminaries

A. Model and notation

To rewrite the measurements (1), we introduce masks $\tilde{m}_j$, $j \in [d]$, given by

$$(\tilde{m}_j)_n := w_n^* e^{\frac{2\pi i(j-1)(n-1)}{d}} \mathcal{I}_{n\le\delta},\ n \in [d],$$

where w^* denotes the complex conjugate transpose of a vector or matrix w and $\mathcal{I}_{\mathcal{C}}$ is 1 when condition $\mathcal{C}$ is true and 0 otherwise. Also, by S_ℓ, $\ell \in \mathbb{N}$, we denote the discrete circular shift operator $S_\ell : \mathbb{C}^d \to \mathbb{C}^d$ defined as $(S_\ell x_0)_j := (x_0)_{\ell+j}$. We consider all indices modulo d, so that x_k should be understood as to $x_{(k-1 \mod d)+1}$. With these definitions the squared magnitude measurements (1) can be expressed as

$$(y_\ell)_j = |\langle S_\ell x_0, \tilde{m}_j\rangle|^2 + n_{j,\ell} = |\langle x_0, S_\ell^* \tilde{m}_j\rangle|^2 + n_{j,\ell}, \quad (2)$$

for all $(j,\ell) \in [d]\times P$. In this paper, we will mainly work with slight modifications of the masks $\tilde{m}_j$, which are obtained by subsampling in frequency domain, i.e., for each $j \in [2\delta-1]$

$$(m_j)_n := \frac{1}{\sqrt[4]{2\delta-1}} w_n^* \cdot e^{\frac{2\pi i(n-1)(j-1)}{2\delta-1}} \mathcal{I}_{n\le\delta},\ n \in [d]. \quad (3)$$

While (3) allows for any window w, we will be particularly interested in Gaussian windows as given by the formula

$$w_n = e^{-\frac{1}{2\sigma^2\delta}\left(n-\frac{\delta+1}{2}\right)^2} \mathcal{I}_{n\le\delta}, \quad n \in [d], \quad (4)$$

which are good approximations of windows appearing in ptychography.

B. Idea of the BlockPR algorithm

The *BlockPR* algorithm [12] consists of the two main steps. Firstly, it establishes a linear system relating the measurements and the lifted object $x_0x_0^*$ and inverts it. Secondly, it reconstructs x_0 from its lifted counterpart. The support size δ plays a crucial role for the algorithm, as it helps to control the dimension blow up by $d(2\delta-1)$ rather than d^2. In this summary we restrict ourselves to the noiseless version of the algorithm. In this case (2) can be transformed as follows.

$$\begin{aligned}(y_\ell)_j &= |\langle x_0, S_\ell^* m_j\rangle|^2 = m_j^* S_\ell x_0 x_0^* S_\ell^* m_j \\ &= \operatorname{tr}(x_0x_0^* S_\ell^* m_j m_j^* S_\ell) = \langle x_0x_0^*, S_\ell^* m_j m_j^* S_\ell\rangle_F,\end{aligned}$$

where $\langle\cdot,\cdot\rangle_F$ denotes the Frobenius inner product defined as $\langle A, B\rangle_F := \operatorname{tr}(A^*B)$.

Also, we only consider the case when all shifts are observed, that is, $P = [d]_0 := \{0,\dots,d-1\}$. Note that since the masks are compactly supported, one has $A_{i,j} = 0$ when $|k-j| < \delta$ or $|k-j| > d-\delta$ for every matrix $A \in \operatorname{span}\left\{S_\ell^* m_j m_j^* S_\ell\right\}_{j\in[K],\ell\in[d]_0}$, meaning that some of the entries of A are not measured. This behavior is captured by the orthogonal projection operator $T_\delta : \mathbb{C}^{d\times d} \to \mathbb{C}^{d\times d}$, $k \in \mathbb{N}$ defined as

$$(T_\delta(A))_{kj} = \begin{cases} A_{k,j} & \text{if } |k-j| < \delta \text{ or } |k-j| > d-\delta, \\ 0, & \text{else.}\end{cases}$$

Indeed, the operator T_δ is an orthogonal projection from the space of all Hermitian $d\times d$ matrices $\mathcal{H}^d$ onto its range $T_\delta(\mathcal{H}^d) \supseteq \operatorname{span}\left\{S_\ell^* m_j m_j^* S_\ell\right\}_{j\in[K],\ell\in[d]_0}$. Consequently,

$$\langle x_0x_0^*, S_\ell^* m_j m_j^* S_\ell\rangle = \langle T_\delta(x_0x_0^*), S_\ell^* m_j m_j^* S_\ell\rangle.$$

Thus the linear operator $\mathcal{A} : \mathcal{H}^d \to \mathbb{C}^D$, $D := d(2\delta-1)$, describing the measurement process is given by

$$\mathcal{A}(X) = \left[\langle X, S_\ell^* m_j m_j^* S_\ell\rangle\right]_{(\ell,j)}$$

and (2) reads as

$$(y_\ell)_j = \left(\mathcal{A}|_{T_\delta(\mathcal{H}^d)} T_\delta\left(x_0x_0^*\right)\right)_{(\ell,j)}.$$

Here $\mathcal{A}|_{T_\delta(\mathcal{H}^d)}$ denotes the restriction of the operator $\mathcal{A}$ to the domain $T_\delta(\mathcal{H}^d)$.

If one can invert $\mathcal{A}|_{T_\delta(\mathcal{H}^d)}$ this yields $X_0 := T_\delta(x_0x_0^*)$. x_0 is then reconstructed from X_0 via angular synchronization [13]: The magnitudes of the entries of x_0 are recovered as square roots of the diagonal elements of X_0. The phases of x_0 are obtained from the entrywise normalization of the top eigenvector of the matrix

$$(\tilde{X}_0)_{k,j} := ((X_0)_{k,j}/|(X_0)_{k,j}|)\cdot \mathcal{I}_{|(X_0)_{k,j}|\neq 0}.$$

The complete reconstruction procedure is summarized in Algorithm 1.

To further improve the Algorithm 1, one can employ Block Magnitude estimation [12], [14], [15] for the magnitude estimation step. This approach provides better reconstruction quality in the presence of noise. It also a part of our implementation.

Algorithm 1: *BlockPR* [12]

Input : Measurements $y \in \mathbb{R}^D$ as in (2)
Output: $x \in \mathbb{C}^d$ with $x \approx e^{-i\theta}x_0$ for some $\theta \in [0, 2\pi]$
1. Compute $X = \left[\mathcal{A}|_{T_\delta(\mathcal{H}^d)}\right]^{-1} y \in T_\delta(\mathcal{H}^d)$.
2. Form $\tilde{X} \in T_\delta(\mathcal{H}^d)$ as $\tilde{X}_{k,j} = X_{k,j}/|X_{k,j}|$.
3. Compute the normalized top eigenvector of $\tilde{X}$, denoted $\tilde{x} \in \mathbb{C}^d$, with $\|\tilde{x}\|_2 = \sqrt{d}$.
4. Set $x_j = \sqrt{X_{j,j}} \cdot (\tilde{x})_j$ for all $j \in [d]$.

III. Results

The backbone of the Algorithm 1 is the invertibility and well-conditioning of the operator $\mathcal{A}|_{T_\delta(\mathcal{H}^d)}$. These properties are determined by the choice of the window w. In [16] the authors prove that the window $w_n = e^{-n/\alpha}\mathcal{I}_{n\leq\delta}$ grants invertibility and the minimal singular value of the measurement operator behaves proportionaly to δ^{-1} when the parameter α is chosen to be $\max\{4, (\delta-1)/2\}$. This results in severe conditioning problems as the support size grows. Further works on this topic [14], [15] extend the range of possible windows, but many windows were not yet covered. The following theorem shows that the measurement operator $\mathcal{A}|_{T_\delta(\mathcal{H}^d)}$ is not even invertible in many cases including Gaussian windows (4).

Theorem 1. *Consider masks of the form* (3)*. Assume that d is even and the window w satisfies the symmetry condition*

$$w_n = w^*_{\delta-n+1} \text{ for all } n \in [\delta].$$

Then, $\mathcal{A}|_{T_\delta(\mathcal{H}^d)}$ is not invertible.

The results of the theorem can be reinterpreted as follows. For symmetric windows, the space spanned by the measurements does not cover $T_\delta(\mathcal{H}^d)$ and thus there exists a nontrivial "lost subspace" $\mathcal{L} \subset T_\delta(\mathcal{H}^d)$ such that $T_\delta(\mathcal{H}^d) = \operatorname{span}\left\{S^*_\ell m_j m^*_j S_\ell\right\}_{j\in[K],\ell\in[d]_0} \oplus \mathcal{L}$. The main idea of this paper is that this subspace can be recovered using the the rank one structure of $x_0x_0^*$. Moreover, this principle can be extended to stabilize the inversion by treating the "approximately lost subspace" corresponding to an ill-conditioned part of the operator $\mathcal{A}|_{T_\delta(\mathcal{H}^d)}$ in a similar way. Our main contribution, Algorithm 2, summarizes this ideas. Its key components are presented in the remainder of this section.

A. Generalized inversion step

For parts of our procedure we vectorize the matrix X_0 and represent the operator $\mathcal{A}|_{T_\delta(\mathcal{H}^d)}$ as a matrix. We will use the same notation for both operator and matrix representations of $\mathcal{A}|_{T_\delta(\mathcal{H}^d)}$.

The SVD of the measurement matrix is denoted by

$$\begin{aligned}\mathcal{A}|_{T_\delta(\mathcal{H}^d)} &= U\Sigma V^* \\ &= \begin{pmatrix} U_1 & U_2 \end{pmatrix} \begin{pmatrix} \Sigma_1 & 0 \\ 0 & \Sigma_2 \end{pmatrix} \begin{pmatrix} V_1 & V_2 \end{pmatrix}^*,\end{aligned}$$

where U and V are unitary matrices and Σ is a diagonal matrix with non-negative entries. Given a threshold $\varepsilon \geq 0$, the singular values are split into two subsets, greater and smaller or equal than ε, denoted by Σ_1 and Σ_2, respectively. We also split right and left singular vectors accordingly. The subspace $\mathcal{S}$ is defined as

$$\mathcal{S} := \operatorname{span}\{V^{(i)} : V^{(i)} \text{ column of } V_1\}.$$

Finally, we define a pseudo-inverse operator as

$$\mathcal{A}|^{-1}_{\mathcal{S}} := \begin{pmatrix} V_1 & V_2 \end{pmatrix} \begin{pmatrix} \Sigma_1^{-1} & 0 \\ 0 & 0 \end{pmatrix} \begin{pmatrix} U_1 & U_2 \end{pmatrix}^*.$$

When $\varepsilon = 0$, this results into $\mathcal{A}|^{-1}_{\mathcal{S}}$ being the Moore-Penrose pseudo inverse matrix and in other cases, ε can be seen as a regularization parameter.

We apply $\mathcal{A}|^{-1}_{\mathcal{S}}$ to the measurements, and denote the resulting estimate by $X_{\mathcal{S}} := \mathcal{A}|^{-1}_{\mathcal{S}} y$. Note that in general $X_{\mathcal{S}} \neq X_0$, when Σ_2 is not empty. The missing part of the information about X_0 will be recovered using the structure of X_0.

B. Subspace Completion Algorithm

The (circular) diagonals L^r , $r \in [2\delta-1]$, of the matrix X_0 are defined entrywise for $z \in [d]$ as

$$L^r_z = \begin{cases} (x_0)^*_z (x_0)_{z+r-1} & \text{if } 1 \leq r \leq \delta, \\ (x_0)^*_{z+1} (x_0)_{z+1+r-2\delta} & \text{if } \delta+1 \leq r \leq 2\delta-1. \end{cases} \tag{5}$$

Each right singular vector of $\mathcal{A}|_{T_\delta(\mathcal{H}^d)}$ is supported on one of these diagonals. Moreover, there is a one to one correspondence between the Fourier coefficients of the diagonals L^r and the right singular vectors, as the next theorem states. Here, by Fourier coefficients we refer to the discrete Fourier transform given by

$$\hat{x}_k := \sum_{n=1}^{d} x_n e^{\frac{-2\pi i(n-1)(k-1)}{d}}, \ x \in \mathbb{C}^d.$$

Theorem 2. *Consider measurement masks of the form* (3)*. Then,*

$$\widehat{L^r}_\xi = \sqrt{d}\, \langle \operatorname{vec}(X_0), V^{(q)} \rangle, \tag{6}$$

where q is decomposed as

$$q = (2\delta-1)(\xi-1) + r$$

with $\xi \in [d]$ and $r \in [2\delta-1]$.

The equality (6) remains true if X_0 is replaced by $X_{\mathcal{S}}$, but only when $V^{(q)} \in \mathcal{S}$. Consequently, one obtains

Corollary 3. *Under the assumption of Theorem 2 in the noiseless case where $X_{\mathcal{S}} = \mathcal{A}|^{-1}_{\mathcal{S}} y$ it holds that*

$$\sqrt{d}\, \langle \operatorname{vec}(X_{\mathcal{S}}), V^{(q)} \rangle = \begin{cases} \widehat{L^r}_\xi & \text{if } V^{(q)} \text{ is a column of } V_1, \\ 0 & \text{if } V^{(q)} \text{ is a column of } V_2 \end{cases}$$

Thus, the lost part of X_0 can be expressed through the missing Fourier coefficients of the diagonals L^r and recovered via the following lemma.

Algorithm 2: Block Phase Retrieval with Subspace Completion (*BlockPR + SC_ε*).

Input : Measurements $y \in \mathbb{R}^D$ as in (2), truncation parameter $\varepsilon \geq 0$

Output: $x \in \mathbb{C}^d$ with $x \approx e^{-i\theta}x_0$ for some $\theta \in [0, 2\pi]$

1. Compute $X_{\mathcal{S}} = \mathcal{A}|_{\mathcal{S}}^{-1} y \in T_\delta(\mathcal{H}^d)$.
2. Evaluate Fourier coefficients of diagonals L^r corresponding to columns of V_1 by Corollary 3.
3. Recover missing entries of $\widehat{L^r}$ by solving (7).
4. Form X with diagonals L^r.
5. Form $\tilde{X} \in T_\delta(\mathcal{H}^d)$ as $\tilde{X}_{k,j} = X_{k,j}/|X_{k,j}|$.
6. Compute the normalized top eigenvector of $\tilde{X}$, denoted $\tilde{x} \in \mathbb{C}^d$, with $\|\tilde{x}\|_2 = \sqrt{d}$.
7. Set $x_j = \sqrt{X_{j,j}} \cdot (\tilde{x})_j$ for all $j \in [d]$.

Lemma 4. *Let L^r and L^ℓ, $r, \ell \in [\delta]$, be diagonals* (5)*. Then, the following relation holds*

$$L^r \circ S_{\ell-1}(L^r)^* = L^\ell \circ S_{r-1}(L^\ell)^*. \tag{7}$$

By solving (7), all diagonals L^r are recovered and X_0 can be formed. The recovery of x_0 from X_0 is identical to Algorithm 1. The full recovery procedure with the lost subspace completion step is summarized in Algorithm 2.

In general equation (7) establishes a quadratic system. However, it is reasonable to assume that at most one Fourier coefficient of each diagonal is missing and then (7) becomes a linear system. Indeed, the singular values corresponding to a single diagonal L^r are given by the function

$$\left| \sum_{\ell=1}^{\delta-r+1} w_\ell^* w_{\ell+r-1} e^{\frac{2\pi i t(\ell-1)}{d}} \right|, \ t \in [0, d),$$

evaluated at integer points. Since this function is highly oscillating, hitting zero at an integer point is a rare event, except for a zero that results from the symmetry for $t = d/2$ on some diagonals. Thus, encountering two zeros on one diagonal is much less common than just one. For the same reason it is commonly the case that on at least one of the diagonals one does not encounter any zeros. This heuristic leads to the assumptions of the following theorem, which are indeed sufficient to guarantee recovery.

Theorem 5. *Assume that*

(A1) *At least one diagonal L^r, $r \neq 1$ is fully recovered in the step 2 of Algorithm 2.*

(A2) *At most one Fourier coefficient of each diagonal is missing.*

Then (7) *can be expressed as a linear system and Algorithm 2 recovers the lost Fourier coefficients via standard solution strategies.*

The numerical experiments presented in the following section confirm that the assumptions (A1) and (A2) are justified in realistic scenarios such as for Gaussian windows and Algorithm 2 yields improved reconstruction quality.

IV. Numerics

In this section we present the results of numerical trials for the evaluation of the performance of Algorithm 2. For the synthetic data generation we use i.i.d. zero-mean complex random multivariate Gaussian vectors. The noise in the measurements (2) is modeled by real Gaussian random variables. The level of noise is measured in decibels (dB) in terms of signal to noise ratios (SNRs), defined as

$$\text{SNR (dB)} = 10 \log_{10} \left(\frac{\sum_{\ell=0}^{d-1} \sum_{j=1}^{2\delta-1} (y_\ell)_j^2}{d(2\delta-1)\nu^2} \right),$$

where $(y_\ell)_j$ are measurements as in (2) and ν^2 denotes the variance of the noise. As an error metric, the minimal relative error between x_0 and its estimate is used, which is given by

$$\min_{\theta \in [0,2\pi]} \left\| x - e^{i\theta} x_0 \right\|_2 / \left\| x_0 \right\|_2 .$$

Each data point of the following figures is the average error obtained by 100 different test signals.

The first example demonstrates the improvement granted by the subspace completion step for a Gaussian window (4) with support size $\delta = 8$ and scaling parameter $\sigma = 0.3$. Figure 1 shows the reconstruction quality for dimension $d = 64$ for both *Block PR* and *Block PR + $SC_{10^{-4}}$*. Since d is even, by Theorem 1 the operator $\mathcal{A}|_{T_\delta(\mathcal{H}^d)}$ is not invertible and the reconstruction with *BlockPR* fails. However, the assumptions (A1) and (A2) are fulfilled and thus Algorithm 2 successfully recovers the lost subspace and accurately reconstructs the signal.

In the second example the effect of the truncation parameter ε is analyzed. In Figure 1 we already observed that Algorithm 2 enables the reconstruction with $\varepsilon = 10^{-4}$ and only has to complete the subspace corresponding to the zero singular values. As it was mentioned above, higher values of ε can be used as a regularization parameter to improve the noise robustness. Figure 2 shows the impact of different values of ε on the reconstruction error for the same setup as in the first example. For comparison reasons, the performance of *Wirtinger Flow* [10] is included.

We observe that by increasing ε the reconstruction at low and medium SNRs improves significantly. On the contrary, the error no longer converges to zero for small noise levels due to the fact that for higher ε assumptions (A1) and (A2) are violated. So solving (7) becomes a harder problem and our solver is not capable of completing the lost information correctly. For $\varepsilon = 10^{-1}$ Table I shows that $2/3$ of the singular values are truncated and the loss of information is too large

TABLE I
Frequency table of the 960 singular values for $d = 64$ and $\delta = 8$ for a Gaussian window with scaling $\sigma = 0.3$.

$\{0\}$	$(10^{-4}, 10^{-3}]$	$(10^{-3}, 10^{-2.5}]$
7	8	22
$(10^{-2.5}, 0.01]$	$(0.01, 0.1]$	$(0.1, 10]$
50	578	295

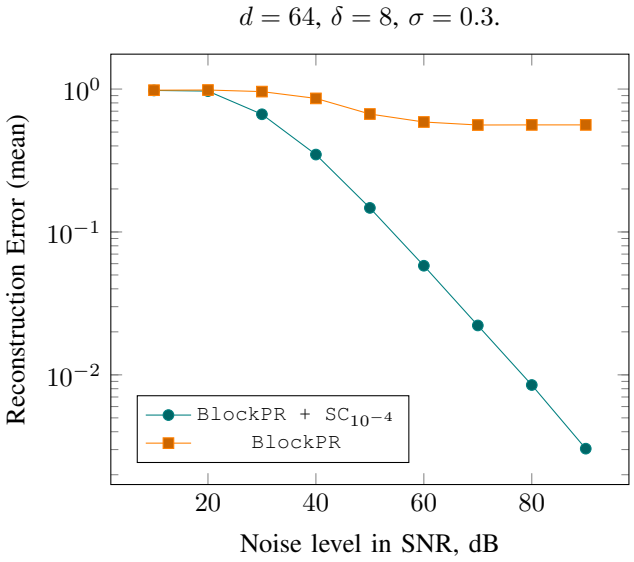

Fig. 1. Comparison of the reconstruction accuracy between the *BlockPR* algorithm and the *BlockPR* + $SC_{10^{-4}}$.

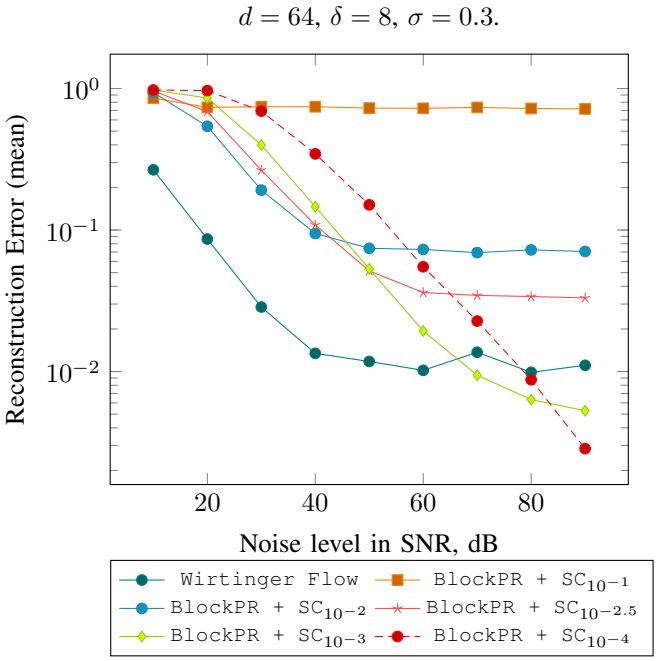

Fig. 2. Comparison of the reconstruction accuracy for different truncation parameters ε for the *BlockPR* + SC_ε algorithm and *Wirtinger Flow* for window size $\delta = 8$ and dimension $d = 64$ (left) and $d = 256$ (right).

making signal reconstruction impossible. Hence, the choice of ε should be made depending on the noise level: large ε leads to noise robustness for low SNRs and small ε grants perfect reconstruction for high SNRs.

Figure 2 also shows one of the core issues of the iterative algorithms. As the noise diminishes, *Wirtinger Flow* stagnates around 1% error without reaching true solution. As one can observe (we omitted the plots due to space constraints), this effect is even amplified for higher dimensions d.

V. Conclusions and Future Work

In this paper, we developed a subspace completion technique to complement the *BlockPR* algorithm, which allows for recovery in ptychography for a larger class of windows. Furthermore, our technique can be used as a regularizer for better noise robustness. The next steps will be the improvement of the solver used for (7). Also, we plan to consider the extension of the technique to models with shifts longer than 1 as proposed in [14] and [17].

Acknowledgment

The authors thank Frank Filbir for many inspiring discussions on the topic.

References

[1] W. Hoppe, "Beugung im inhomogenen primärstrahlwellenfeld. iii. amplituden- und phasenbestimmung bei unperiodischen objekten," *Acta Crystallographica Section A*, vol. 25, no. 4, pp. 508–514, 1969.

[2] R. Bates and J. M. Rodenburg, "Sub-ångström transmission microscopy: A fourier transform algorithm for microdiffraction plane intensity information," *Ultramicroscopy*, vol. 31, no. 3, pp. 303–307, 1989.

[3] B. McCallum and J. Rodenburg, "Two-dimensional demonstration of wigner phase-retrieval microscopy in the stem configuration," *Ultramicroscopy*, vol. 45, no. 3-4, pp. 371–380, 1992.

[4] J. M. Rodenburg, B. C. McCallum, and P. D. Nellist, "Experimental tests on double-resolution coherent imaging via stem," *Ultramicroscopy*, vol. 48, no. 3, pp. 304–314, 1993.

[5] A. Sakdinawat and D. Attwood, "Nanoscale x-ray imaging," *Nature Photonics*, vol. 4, no. 12, pp. 840–848, 2010.

[6] da Silva et al., "Assessment of the 3 d pore structure and individual components of preshaped catalyst bodies by x-ray imaging," *ChemCatChem*, vol. 7, no. 3, pp. 413–416, 2015.

[7] V. Piazza, B. Weinhausen, A. Diaz, C. Dammann, C. Maurer, M. Reynolds, M. Burghammer, and S. Köster, "Revealing the structure of stereociliary actin by x-ray nanoimaging," *ACS Nano*, vol. 8, no. 12, pp. 12 228–12 237, 2014.

[8] R. W. Gerchberg, W. O. Saxton, "A practical algorithm for the determination of phase from image and diraction plane pictures," *Optik*, no. 35, pp. 237–246, 1972.

[9] J. R. Fienup, "Reconstruction of an object from the modulus of its fourier transform," *Optics letters*, vol. 3, no. 1, pp. 27–29, 1978.

[10] E. J. Candes, X. Li, and M. Soltanolkotabi, "Phase retrieval via wirtinger flow: Theory and algorithms," *IEEE Transactions on Information Theory*, vol. 61, no. 4, pp. 1985–2007, 2015.

[11] A. M. Maiden and J. M. Rodenburg, "An improved ptychographical phase retrieval algorithm for diffractive imaging," *Ultramicroscopy*, vol. 109, no. 10, pp. 1256–1262, 2009.

[12] M. A. Iwen, B. Preskitt, R. Saab, and A. Viswanathan, "Phase retrieval from local measurements: Improved robustness via eigenvector-based angular synchronization," vol. 2016. [Online]. Available: http://arxiv.org/pdf/1612.01182v2

[13] A. Singer, "Angular synchronization by eigenvectors and semidefinite programming," *Applied and Computational Harmonic Analysis*, vol. 30, no. 1, pp. 20–36, 2011.

[14] B. Preskitt and R. Saab, "Admissible measurements and robust algorithms for ptychography." [Online]. Available: http://arxiv.org/pdf/1910.03027v1

[15] B. P. Preskitt, "Phase retrieval from locally supported measurements. phd thesis uc san diego," 2018. [Online]. Available: https://escholarship.org/uc/item/97v5k8j9

[16] M. A. Iwen, A. Viswanathan, and Y. Wang, "Fast phase retrieval from local correlation measurements," *SIAM Journal on Imaging Sciences*, vol. 9, no. 4, pp. 1655–1688, 2016.

[17] Oleh Melnyk, Frank Filbir, Felix Krahmer, "Phase retrieval from local correlation measurements with fixed shift length," Sampling Theory & Applications (2019). [Online]. Available: https://sampta2019.sciencesconf.org/272661/document